Cell Transplantation, Vol. 24, pp. 2643–2655, 2015

0963-6897/15 $90.00 + .00
DOI: http://dx.doi.org/10.3727/096368915X687219
E-ISSN 1555-3892
www.cognizantcommunication.com

Systemic and Local Administration of Allogeneic Bone Marrow-Derived Mesenchymal Stem Cells Promotes Fracture Healing in Rats

Shuo Huang,*†‡[1] Liangliang Xu,*†‡[1] Yifeng Zhang,*† Yuxin Sun,*†‡ and Gang Li*†‡§

*Department of Orthopaedics and Traumatology, Li Ka Shing Institute of Health Sciences, The Chinese University of Hong Kong, Prince of Wales Hospital, Shatin, Hong Kong, PR China
†Lui Che Woo Institute of Innovative Medicine, Faculty of Medicine, The Chinese University of Hong Kong, Prince of Wales Hospital, Shatin, Hong Kong, PR China
‡The Chinese University of Hong Kong Shenzhen Research Institute, Shenzhen, PR China
§Key Laboratory for Regenerative Medicine, Ministry of Education, School of Biomedical Sciences, Faculty of Medicine, The Chinese University of Hong Kong, Hong Kong SAR, China

Mesenchymal stem cells (MSCs) are immune privileged and a cell source for tissue repair. Previous studies showed that there is systemic mobilization of osteoblastic precursors to the fracture site. We hypothesized that both systemic and local administration of allogeneic MSCs may promote fracture healing. Bone marrow-derived MSCs and skin fibroblasts were isolated from GFP Sprague–Dawley rats, cultured, and characterized. Closed transverse femoral fracture with internal fixation was established in 48 adult male Sprague–Dawley rats, which were randomly assigned into four groups receiving PBS injection, MSC systemic injection, fibroblast systemic injection, and MSC fracture site injection; 2×10^6 cells were injected at 4 days after fracture. All animals were sacrificed at 5 weeks after fracture; examinations included weekly radiograph, micro-CT, mechanical testing, histology, immunohistochemistry, and double immunofluorescence. The callus size of MSC injection groups was significantly larger among all the groups. Radiographs and 3D reconstruction images showed that the fracture gaps united in the MSC injected groups, while gaps were still seen in the fibroblast and PBS injection groups. The mechanical properties were significantly higher in the MSC injection groups than those in the fibroblast and PBS groups, but no difference was found between the MSC local and systemic injection groups. Immunohistochemistry and double immunofluorescence demonstrated that GFP-positive MSCs were present in the callus in the MSC injection groups at 5 weeks after fracture, and some differentiated into osteoblasts. Quantitative analysis revealed the number of GFP-positive cells in the callus in the MSC systemic injection group was significantly lower than that of the MSC local injection group. The proportion of GFP osteoblasts in GFP-positive cells in the MSC systemic injection group was significantly lower than that of the MSC local injection group. These findings provide critical insight for developing MSC-based therapies, and systemic injection of allogeneic MSCs may be a novel treatment method for promoting fracture repair.

Key words: Allogeneic mesenchymal stem cells (MSCs); Systemic injection; Local injection; Fracture healing

INTRODUCTION

Mesenchymal stem cells (MSCs) are multipotent stem cells that have the potential to self-renew and differentiate into a variety of specialized cell types such as osteoblasts, chondrocytes, adipocytes, cardiomyocytes, and neurons (32,33). MSCs can be isolated from various sources such as adipose tissue, tendons, peripheral blood, cord blood, fetus (1,6,14,35), and bone marrow (BMMSCs) as the most common source of MSCs. MSCs are also easily culture expanded, immune privileged, and they do not elicit immediate immune responses (18,20). Therefore, MSCs are attractive cell sources for tissue repairing and engineering and vehicles of cell-based gene therapy.

Studies in animal models have demonstrated the potential use of MSCs for cell therapies in various diseases. Chen et al. showed that MSCs are a promising cell resource for cardiac repair. MSC administration significantly increased the left ventricular ejection fraction (10). Lee et al. observed that in human MSC-treated diabetic mice, there was an increase in pancreatic islets and β-cells

Received November 13, 2014; final acceptance January 23, 2015. Online prepub date: February 2, 2015.
[1]These authors provided equal contribution to this work.
Address correspondence to Gang Li, M.B.B.S., D. Phil. (Oxon), Li Ka Shing Institute of Health Institute, Prince of Wales Hospital, The Chinese University of Hong Kong, Room 904, 9/F, Shatin, Hong Kong, SAR, PR China. Tel: (+852) 3763 6153; Fax: (+852) 2646 3020; E-mail: gangli@cuhk.edu.hk

producing mouse insulin (23). Parekkadan et al. reported that extracorporeal perfusion with a bioreactor containing MSCs could provide a significant survival benefit in rats undergoing fulminant hepatic failure (31). Intravenous infusion of autologous MSCs to stroke patients is a feasible and safe therapy that may improve functional recovery (2,22). MSCs have been also tried for treatment of lung injuries. Ortiz et al. showed that murine MSCs home to the lung in response to bleomycin-induced injury and reduce inflammation and collagen deposition in lung tissue (29,30). There is much compelling evidence that MSCs can repair bone and related defects in many animal models (4,5,25). MSCs are also a promising cell source for bone tissue engineering (13,15). In 2005, Shirley et al. reported that there was a systemic mobilization and recruitment of osteoblastic precursors to the fracture site via the peripheral circulation (34). We therefore hypothesized that systemic and local administration of allogeneic MSCs may promote fracture healing.

MATERIALS AND METHODS

Chemicals

The chemicals used were all purchased from Sigma-Aldrich (St. Louis, MO, USA) except where specified.

Isolation and Cultivation of Rat BMMSCs

All animal experiments were approved by the Animal Research Ethics Committee of the authors' institution. Eight-week-old male Sprague–Dawley (SD) rats that overexpress green fluorescent protein (GFP-rat; Japan SLC Inc., Japan) were sacrificed by intramuscular injection of overdose pentobarbital sodium (Vedco Inc., St. Joseph, MO, USA). Femurs were dissected, muscle and connective tissues were removed, and then femurs were stored on ice in phosphate-buffered saline (PBS; Sigma-Aldrich) with 1% penicillin–streptomycin–neomycin (PSN) (Sigma-Aldrich). Under the laminar flow in a biological safety cabinet, two ends of the femurs were excised, and the marrow cavity was repeatedly flushed by 10 ml Alpha complete culture medium with 10% fetal bovine serum (Life Technologies, Grand Island, NY, USA) and 1% PSN. Ten milliliters of marrow suspension was carefully layered over 5 ml Lymphoprep™ (Stemcell Technologies Inc., Vancouver, Canada) in a 50-ml centrifuge tube (Cat. No. CFT012500; Guangzhou Jet Bio-Filtration Products Co., Ltd., Gaungzhou, China), then centrifuged at 800 × *g* for 20 min at room temperature. After centrifugation, a distinct band containing mononuclear cells at the medium interface was formed. Cells were then carefully removed from the interface by pipette without disturbing the upper layer. The harvested cells were diluted with 5 ml DMEM culture medium (Invitrogen Corporation, Carlsbad, CA, USA) and centrifuged at 800 × g for 5 min. Then cells were cultured in a 100-mm cell culture dish (Product No. 353803; Corning Life Sciences, Corning, NY, USA) in the DMEM culture medium with 10% fetal bovine serum at 37°C with 5% CO_2 and 95% humidity. The adherent spindle-shaped cells appeared at around the third day. At 80–90% confluence, cells were harvested with 2.5% trypsin (Sigma-Aldrich) and replated by splitting at a ratio of 1:3 into 75-cm^2 cell culture flasks (No. 430641; Corning Life Sciences). After three passages, a homogeneous cell population was obtained. MSCs at passage 5 were used in this study. MSC markers CD44 (BD Pharmingen, Franklin Lakes, NJ, USA), CD90 (BD Biosciences, San Jose, CA, USA), endothelial cell marker CD31 (BD Biosciences), and hematopoietic marker CD34 (BD Biosciences) were examined by flow cytometry. Briefly, 1×10^5 harvested cells were stained with 1 µg/100 µl fluorescent phycoerythrin (PE)-conjugated CD31, CD34, CD44, and CD90 (all from BD Biosciences) for 1 h at 4°C. The cells stained with PE-labeled IgG served as controls. Then the cells were pelleted, washed twice with PBS, and resuspended in 0.5 ml stain buffer (BD Pharmingen) for flow cytometric analysis. WinMDI 2.9 software (The Scripps Research Institute, La Jolla, CA, USA) was used to create the histograms. The trilineage differentiation abilities were characterized by Alizarin red, Oil red O, and Safranin-O/fast green (all from Sigma-Aldrich) staining after the corresponding osteogenic, adipogenic, and chondrogenic inductions according to our previously published article (36).

Isolation and Cultivation of Rat Skin Fibroblast

Skin pieces of dimension 1 cm × 1 cm were removed from the GFP-rats. The subcutaneous tissues were removed by scraping the dermal side, and skin samples were cut into tiny pieces with a sharp scalpel. The samples were washed and incubated in 5 ml PBS containing 2.5% trypsin at 37°C for 30 min. Then 5 ml of culture medium was added and centrifuged at 800 × *g* for 5 min; the supernatant was then removed, and pellets and skin pieces were resuspended in the 100-mm cell culture dish and cultured at 37°C with 5% CO_2 and 95% humidity. The fibroblast outgrowth was checked every 3 to 4 days until 80–90% confluence; the cells were then harvested with 2.5% trypsin and replated by splitting into 75-cm^2 cell culture flasks at a ratio of 1:3. At last, the trilineage differentiation abilities were also tested as above.

Animal Details

Forty-eight Sprague–Dawley male rats (14 weeks old, body weight 430–480 g) were used. All rats were obtained from the Laboratory Animal Services Centre of the Chinese University of Hong Kong and housed in a designated, government-approved animal facility at The Chinese University of Hong Kong in accordance with

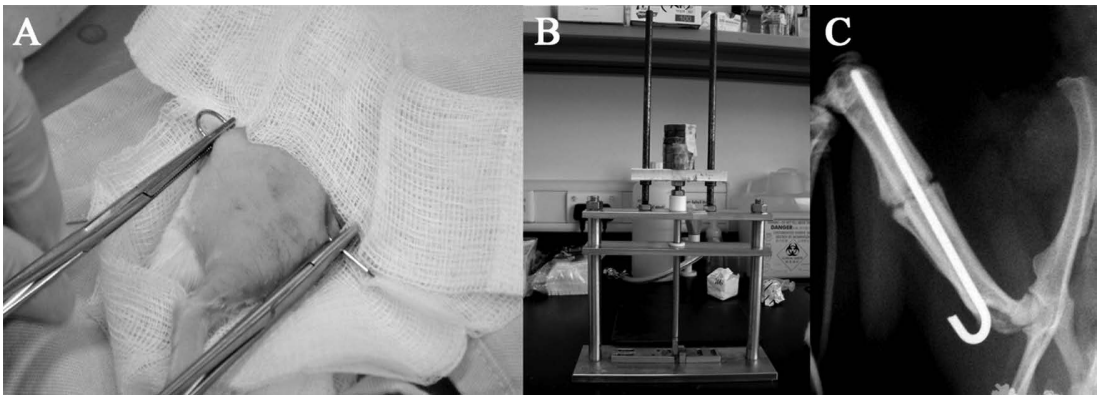

Figure 1. Illustration of rat closed transverse femoral fracture surgery. (A) The rat was anesthetized, a hole was drilled at the intercondylar notch using an 18-gauge needle, a K-wire was inserted into the right femoral bone marrow cavity at the knee level for stabilizing the impending fracture, and the incision was then closed. (B) The closed fracture was produced on the right femur by the three-point bending device. (C) A radiograph was then taken to confirm the fracture.

The Chinese University of Hong Kong's animal experimental regulations.

Animal Surgery

A standard rat closed transverse femoral fracture model with internal fixation was used. Under general anesthesia and sterile conditions, a small incision was made at the knee level. A hole was drilled at the intercondylar notch using an 18-gauge needle (Terumo Corporation, Tokyo, Japan). A K-wire (diameter: 1.2 mm; Stryker Ltd., Kalamazoo, MI, USA) was inserted into the right femoral bone marrow cavity at the knee level (Fig. 1A). The incision was closed, and a closed fracture was produced at the midshaft of the right femur using a custom-made three-point bending device, with a metal blade (weighted 500 g) dropping from a height of 35 cm (Fig. 1B). A radiography was then taken to confirm the fracture (Fig. 1C). Following the surgery, the 48 rats were randomly assigned into four groups: two treatment groups and two control groups, with 12 rats per group (details are shown in Table 1).

Radiography Examination

Weekly X-rays were taken at the day of the fracture surgery and thereafter until sacrifice. For taking X-rays, all animals were anesthetized and placed inside a high-resolution digital radiograph system (Faxitron MX-20 with DC-2 option; Faxitron Bioptics, LLC, Tucson, AZ, USA) using an exposure of 32 kV for 10 s. The callus widths of fractured femurs were determined from radiographs by Image-Pro Plus software (Version 5.0; Media Cybernetics, Inc., Bethesda, MD, USA) (11). The callus width is defined as the maximal outer diameter of the callus minus the corresponding diameter of the femur (11).

Microcomputer Tomography (Micro-CT) Examination

All 48 rats were terminated by intramuscular injection of overdose pentobarbital sodium (Vedco, Inc.) weeks after fracture. Eight rats per group were randomly chosen for micro-CT analysis. Both femurs of all 48 rats were excised; muscles, soft tissues, and the internal K-wires were carefully removed. All femurs were stored in a container humidified by saline-moistened gauze at 4°C before scanning. For image acquisition, a total of 500 two-dimensional (2D) microtomographic slices with a 20-μm slice increment covering a total range of 10 mm were scanned by Scanco Medical Viva CT40 (Scanco Medical AG, Brüttisellen, Switzerland). Four hundred sequential slices of 2D CT images at 4 mm proximal and

Table 1. Animal Experimental Groups (Injection at 4 Days Following Fracture)

Group (12 Rats per Group)	Injection Dose	Injection Site
PBS injection group (4-week normal control)	0.5 ml PBS	Intracardiac injection
MSC systemic injection group (MSC-Sys) (4-week MSC systemic treatment)	2×10^6 GFP-MSCs in 0.5 ml PBS	Intracardiac injection
Fibrolast injection group (4-week fibrolast control)	2×10^6 GFP-Fibroblasts in 0.5 ml PBS	Intracardiac injection
MSC local injection group (MSC-loc) (4-week MSC local treatment)	2×10^6 GFP-MSCs in 0.5 ml PBS	Fracture site injection

4 mm distal to the fracture line were selected, and the contoured region including the cortical diaphyseal bone and endosteal callus was set in each image. A low-pass Gaussian filter (Gauss $\sigma = 0.8$, Gauss support = 1) was used to partly suppress the noise in the volumes. The high and low radio-opacity mineralized tissues were segmented by thresholding, and an appropriate threshold was determined from the gray scale CT images. Newly formed callus (the low-density bone) was considered at threshold 120–320 (low attenuation = 120; high attenuation = 320, in per mille of maximal image gray value); old cortical bone and highly mineralized callus (high-density bone) were considered at 321–1,000, and the unmineralized tissue was considered at 0–119. The same parameters were used for all samples in the study. Three-dimensional evaluations of newly formed callus (threshold at 120–320) and newly formed callus plus high-density bone (threshold at 120–1,000) were separately performed on the basis of microtomographic data sets generated by direct 3D morphometry; bone volume (BV), tissue volume (TV), BV/TV, and mean volumetric bone mineral density (BMD) for each sample were recorded. The 3D reconstruction images of the femurs including fracture site (threshold at 120–1,000) was also performed using the software provided.

Four-Point Bending Mechanical Testing

Tests were performed within 24 h postexcision at room temperature; pair specimens were tested to failure with a constant displacement rate of 5 mm/min by four-point bending device (H25KS; Hounsfield Test Equipment Ltd., Redhill, Surrey, UK). The femurs were loaded in the anterior–posterior direction with the inner and outer span of the blades set as 8 and 20 mm, respectively. The long axis of the femora was oriented perpendicular to the blades during the test (24). After testing, the load–displacement curves of the femurs were generated by the built-in software (QMAT Professional Material testing software; Hounsfield Test Equipment Ltd.); ultimate load to failure, energy absorbed to failure (the area under the load–displacement curves, known as the toughness) (12), and the modulus of elasticity (E-modulus, the slope of the stress–strain curve, known as the tissue stiffness) (12) were recorded and analyzed by the software. The biomechanical properties of the healing fractures were expressed as percentages of the contralateral intact bone properties.

Histology (Hematoxylin and Eosin Staining)

The fractured femurs were fixed in 4% buffered formalin for 1 day and then decalcified with 9% formic acid for 5–7 days. Attempts were made to standardize the sectioning at a midsagittal plane of each specimen by cutting the specimen in half (longitudinally in a sagittal plane) using a slicing blade. Samples were subjected for tissue processing and then embedded in paraffin. Thin sections (7 μm) were cut on a rotary microtome (HM 355S; Thermo Fisher Scientific, Inc., Waltham, MA, USA) along the long axis of each femur in sagittal plane. Sections were mounted on the coated slides. Paraffin was removed by immersing the slides in xylene, two changes of 5 min at room temperature. Slides were then taken through graded ethanol and distilled water, then stained with hematoxylin and eosin (H&E), and at last dehydrated and mounted.

Immunohistochemistry (HRP-DAB Staining for GFP)

The localizations of the GFP-MSCs in the fractured bone were determined by horseradish perioxidase-3, 3'-diaminobenzidine (HRP-DAB) staining. Briefly, antigen retrieval was done by immersing deparaffinized sections into 10 mM of citrate buffer at 60°C for 20 min. Sections were blocked by 5% goat serum in 1% BSA for 20 min, then incubated with the rabbit anti-GFP antibody (1:300; Santa Cruz Biotechnology, Santa Cruz, CA, USA) overnight at 4°C. Sections were washed with PBS three times and incubated in 0.3% H_2O_2 in PBS for 15 min to suppress endogenous peroxidase activity and reduce background staining, then rinsed in PBS three times. Sections were incubated with the goat anti-rabbit-IgG-HRP (1:300; Santa Cruz) for 60 min at room temperature, and the signal was developed by incubating with DAB (Dako Denmark A/S, Glostrup, Denmark) for 1 min. At last, stained slices were counterstained with hematoxylin, dehydrated, mounted, and then observed under the light microscope.

Immunofluorescence Staining for GFP

Briefly, antigen retrieval was done by immersing deparaffinized sections into 10 mM of citrate buffer at 60°C for 20 min. Sections were blocked by 5% goat serum in 1% BSA for 20 min, then incubated with the rabbit anti-GFP antibody (1:300; Life Technologies) overnight at 4°C. Sections were washed with PBS three times, then incubated with the goat anti-rabbit IgG-FITC (1:1,000; Santa Cruz) for 60 min at room temperature in the dark; they were mounted by fluoroshield mounting medium with 4',6-diamidino-2-phenylindole (DAPI; Dako Denmark A/S). Samples were observed and imaged using a fluorescent microscope (Zeiss-spot; Carl Zeiss MicroImaging GmbH, Jena, Thuringia, Germany).

Double Immunofluorescence Staining

As the methods above, after sections were incubated with the secondary antibody, goat anti-rabbit IgG-FITC (1:1,000; Santa Cruz) for 60 min at room temperature in the dark, sections were washed with PBS three times, and then counterstained with the rabbit anti-osterix antibody (1:300; Abcam, Cambridge, UK) or the rabbit anti-nestin antibody (1:300; Sigma-Aldrich) for 1 h at room temperature in the dark,

then washed with PBS three times, and incubated with Cy3 goat anti-rabbit IgG (1:1,000; Life Technologies) for 60 min at room temperature in the dark. They were mounted and observed using the fluorescent microscope.

Quantification of Injected GFP-Positive Cells in the Fracture Site

The immunofluorescence image with the maximum callus width in each sample was chosen for cell counting. Briefly, the image was opened by ImageJ version 1.48 (National Institutes of Health, Bethesda, MD, USA); when the "Plugins/Analyze/Cell Counter" plugin is run, the crosshair (mark and count) tool is used to manually count immunofluorescence-labeled cells. The cell counting result is then generated by the software.

Statistical Analysis

All quantitative data were transferred to statistical spreadsheets and analyzed by a commercially available statistical program SPSS version 16.0 (IBM, Armonk, NY, USA). One-way analysis of variance (ANOVA) followed by Tukey's post hoc test were used for comparison of mean values with $p<0.05$ considered statistically significant.

RESULTS

The Characterization of MSCs and Skin Fibroblasts

The flow cytometry results confirmed that isolated BMMSCs were homogenously positive for MSC markers: CD44 and CD90 (Fig. 2A, B), but negative for the endothelial cell marker CD31 (Fig. 2C) and the hematopoietic marker CD34 (Fig. 2D). In differentiation assays of BMMSCs, the Alizarin red staining demonstrated that mineralized nodules formed after 4 weeks of the osteogenic induction; intracellular Oil red O-stained lipid-rich vacuoles appeared after 2 weeks of the adipogenic induction; sulfated glycosaminoglycan matrix depositions were observed when stained by Safranin-O/fast green after the chondrogenic induction. In contrast, isolated skin fibroblasts did not show these trilineage differentiation abilities (data not shown).

Radiographic Analysis

As shown in the serial radiographs (Fig. 3A), the gaps at fracture sites gradually decreased with the fracture healing process during weekly X-ray follow-up. After 4 weeks following the injections, smaller fracture gaps were found in MSC injection groups (MSC systemic and MSC local), compared to the controls (PBS control and fibroblast control).

Quantitative analysis showed that the mean callus width of fractured femurs in the MSC systemic injection group was significantly larger than that of the PBS control group ($p=0.038$) and the fibroblast injection group ($p=0.029$); the MSC local injection group was also significantly larger than that of the PBS control group ($p=0.019$) and the fibroblast control group ($p=0.015$). There was no significant difference between the MSC systemic and the local injection groups ($p=0.991$). There was no significant difference between the PBS and fibroblast control groups ($p=0.999$) (Fig. 3B).

Micro-CT Analysis of the Fractured Bone

Four representative 3D reconstruction images of the fractured bones (threshold at 320–1,000) by micro-CT from each group showed that fracture gaps were smaller in MSC injection groups (systemic and local), compared to the controls (PBS and fibroblast) (Fig. 3C).

Quantitative analysis revealed that the mean percentage of bone volume over tissue volume (BV/TV) (threshold at 320–1,000) in the MSC systemic injection group was significantly higher than that of the PBS control group ($p=0.017$) and the fibroblast injection group ($p=0.014$). BV/TV (threshold at 320–1,000) in the MSC local injection group was significantly higher than that of the PBS control group ($p=0.038$) and the fibroblast injection group

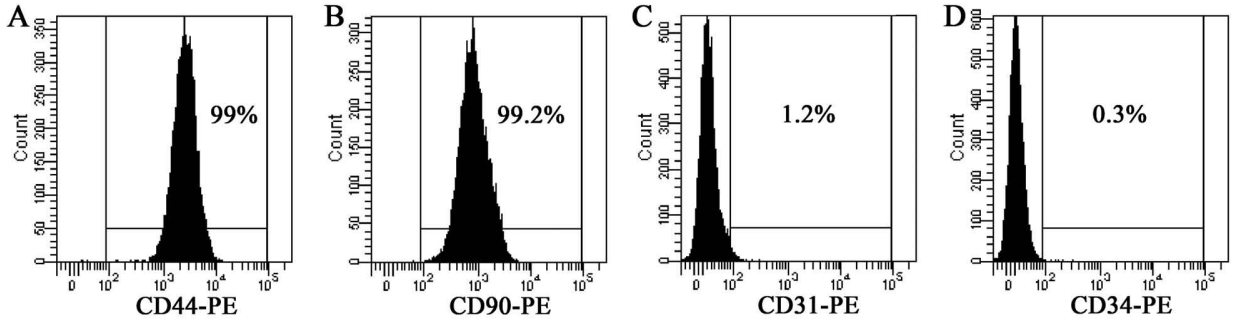

Figure 2. Immunophenotypic characterization of rat mesenchymal stem cells. (A, B) Flow cytometry analysis results confirmed that isolated BMMSCs were positive for mesenchymal stem cell markers CD44 and CD90. (C) Cells were negative for endothelial cell marker CD31. (D) Cells were negative for hematopoietic marker CD34.

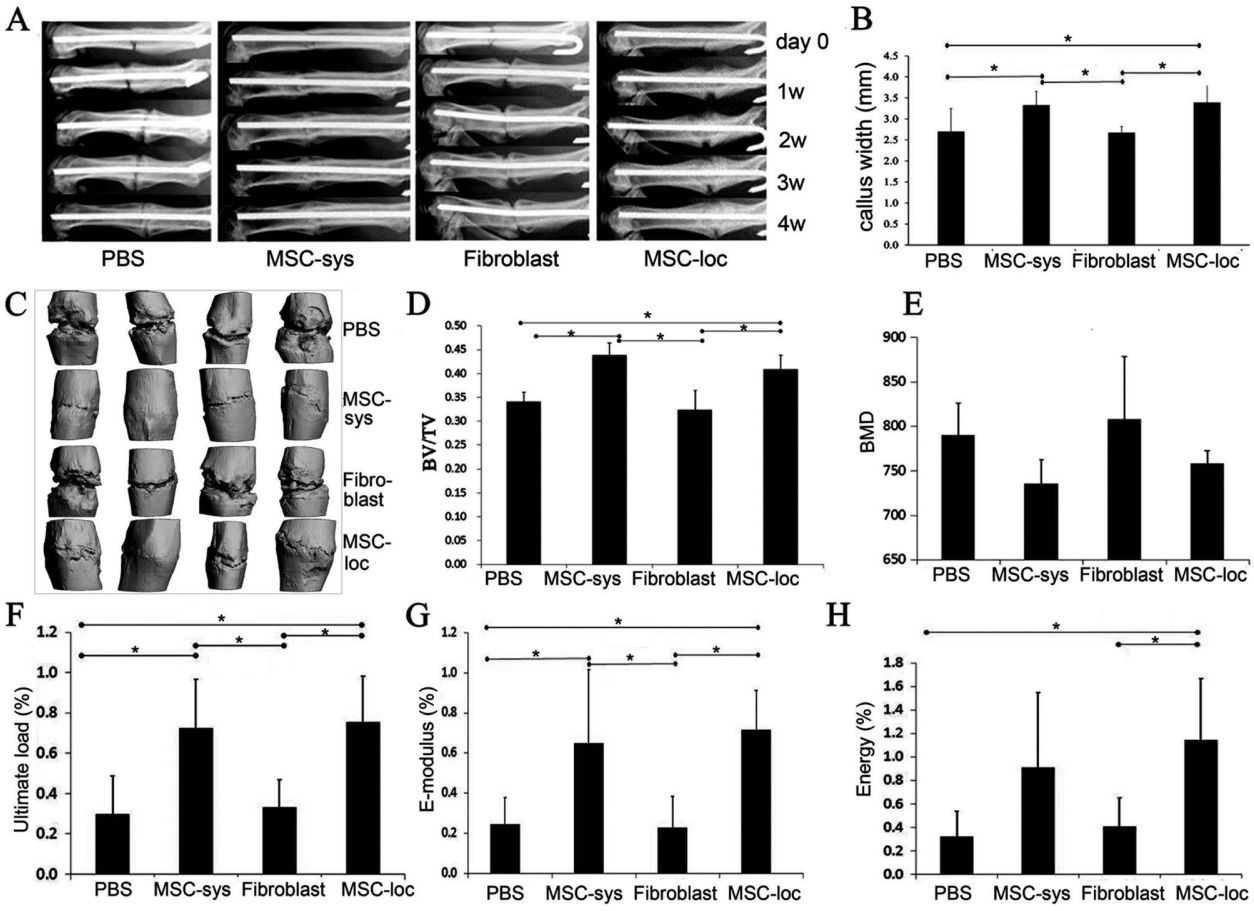

Figure 3. Radiograph, micro-CT, and four-point bending mechanical testing results. (A) Series of representative lateral radiographic pictures among four groups at five different time points (injection days 1, 2, 3, and 4 weeks following the fracture) showed that MSC injection groups (MSC-sys and MSC-loc) had smaller fracture gaps than controls (PBS and fibroblast). (B) The mean callus width of fractured femurs in MSC injection groups was significantly larger than controls. (C) Four representative 3D reconstruction images of the fractured bone by micro-CT from each group showed that fracture gaps were smaller in MSC injection groups compared to the control groups. (D) The micro-CT analysis data showed that BV/TV in MSC injection groups was significantly higher than that in the control groups. (E) The overall BMD at the fracture sites did not show significant difference among the four groups ($p > 0.05$). Four-point bending mechanical testing results showed that ultimate load to failure (F) and E-modulus (G) in the MSC-Sys and MSC-loc injection group were all significantly higher than those in the PBS control group and the fibroblast group. (H) Energy absorbed to failure in the MSC-loc injection group was significantly higher than that of the PBS control group and the fibroblast group. Overall, in all tests, there was no significant difference between MSC-Sys and MSC-loc group, the PBS, and the fibroblast group.

($p = 0.029$), but there was no significant difference between the MSC systemic injection group and the MSC local injection group ($p = 0.293$), the PBS control group and the fibroblast injection group ($p = 0.739$) (Fig. 3D). The overall BMD at the fracture sites did not show significant differences among the four groups ($p > 0.05$) (Fig. 3E).

Four-Point Bending Mechanical Testing

The values of the ultimate load to failure in the MSC systemic injection group was significantly higher than that of the PBS control group ($p = 0.008$) and the fibroblast group ($p = 0.014$). Similarly, the MSC local injection group was significantly higher than that of the PBS control group ($p = 0.004$) and the fibroblast group ($p = 0.008$). However, there was no significant difference in the values of the ultimate load to failure between the MSC systemic injection group and the MSC local injection group ($p = 0.994$); no difference was seen in the PBS control group and the fibroblast injection group ($p = 0.992$) (Fig. 3F).

E-modulus (known as the tissue stiffness) in the MSC systemic injection group was significantly higher than that of the PBS control group ($p = 0.031$) and the fibroblast group ($p = 0.024$), while the MSC local injection group was significantly higher than that of the PBS control group ($p = 0.011$) and the fibroblast group ($p = 0.008$),

but there was no significant difference between the MSC injection groups ($p=0.960$), the PBS control, and the fibroblast injection group ($p=0.998$) (Fig. 3G).

Energy absorbed to failure (known as the toughness) in the MSC local injection group was significantly higher than that of the PBS control group ($p=0.021$) and the fibroblast group ($p=0.042$), but there was no significant difference among the MSC systemic injection group, the fibroblast group, and the PBS group ($p>0.05$) (Fig. 3H).

Histology and Immunostaining for GFP

Representative sections from four groups were stained with H&E. On the H&E histological sections, the amount of new bone and cartilage appeared to be greater in the two MSC-treated groups compared to the fibroblast or PBS-treated groups (Fig. 4A–D). In order to detect the GFP-positive cells, immunostaining was carried out on the paraffin sections using anti-GFP antibody. GFP-positive cells (brown cells) were found in the MSC systemic injection group (Fig. 4E) and MSC local injection group (Fig. 4F) at 5 weeks following the fracture. In contrast, none of GFP-positive cells were found in the fibroblast control group (Fig. 4G) and PBS control group (Fig. 4H). Immunofluorescence staining results showed that GFP-positive cells (green) were found in the MSC systemic injection group (Fig. 4I) and the MSC local injection group (Fig. 4J) at 5 weeks following the fracture, but none of the GFP-positive cells were found in the fibroblast and PBS control group (Fig. 4K, L).

Attempts were also made to locate the injected cells in all samples. We found that GFP-positive cells mainly distributed within the three green outlined areas in both the MSC systemic injection group (Fig. 4E) and the MSC local injection group (Fig. 4F); areas 1 and 3 (Fig. 4E, F) were located at the junctional zone between the newly formed mineralized bone and the cartilage within the callus, and area 2 (Fig. 4E, F) was essentially located at the extension line of the fracture line in the callus. However, different samples have different proportions of GFP-positive cells in three areas. In some samples, GFP-positive cells may be only shown in one or two areas.

Double Immunofluorescence Staining for GFP/Nestin and GFP/Osterix

In order to examine the codistribution of GFP (FITC immunolabeling) and nestin (Cy3 immunolabeling), which is an MSC marker, double immunofluorescence stainings were carried out in the same section. GFP^+/$nestin^+$ MSCs, the red-yellow cells pointed out by red arrows in Figure 5A were observed in the MSC-Sys group, which meant that some systemic injected allogenic GFP-MSCs were able to migrate to the fracture site via system circulation and maintained their phenotype at 5 weeks following the fracture. GFP^+/$nestin^-$ cells, the green cells pointed out by white arrows in Figure 5A, were also observed, which meant that some of the injected GFP-MSCs differentiated into other cell types. GFP-MSCs, GFP^+/$nestin^+$ MSCs (the red-yellow cells pointed out by green arrows in Fig. 5B) were observed in the MSC-loc group at 5 weeks following the fracture. GFP^-/$nestin^+$ MSCs (the red cells pointed out by white arrows in Fig. 5B) were also observed, which meant that autologous MSCs also contribute to the fracture healing. In contrast, GFP-positive cells were not observed in the antibody negative control (without GFP antibody) (Fig. 5C), the PBS control group (Fig. 5D), and the fibroblast group (Fig. 5E), but GFP^-/$nestin^+$ MSCs were found both in the PBS control group and the fibroblast group (red cells pointed out by white arrows in Fig. 5D, E), which meant that autologous MSCs can migrate to the fracture site in control groups.

Double immunofluorescence staining was also carried out to examine the codistribution of GFP (FITC immunolabeling) and osterix (Cy3 immunolabeling), which is a transcription factor for osteoblasts. GFP^+/$osterix^+$ osteoblasts, the red-yellow cells pointed out by white arrows in Figure 6A and B, were observed both in the MSC systemic and local injection groups at 5 weeks following the fracture, which meant that some of the injected GFP-MSCs had already differentiated into osteoblasts and contributed to the fracture healing. GFP^+/$osterix^-$ cells, the green cells pointed out by red arrows in Figure 6A and B, were also found in both systemic and local injection groups, which meant that some injected MSCs could still maintain their phenotype at 5 weeks following the fracture. GFP-positive cells were not observed in the antibody negative control (without GFP antibody) (Fig. 6C), the PBS control group (Fig. 6D), and the fibroblast group (Fig. 6E), but GFP^-/$osterix^+$ osteoblasts were found both in the PBS control group and the fibroblast group (red cells pointed out by white arrows in Fig. 6D, E), which meant that autologous osteoblasts were in the fracture site at 5 weeks following the fracture and contributed to the bone formation in the control groups.

The Number of Injected Cells in the Fracture Site

Quantitative analysis revealed that the number of GFP-positive cells in the callus in the MSC systemic injection group was significantly lower than that of the MSC local injection group (135.3 ± 26.7 vs. 229.3 ± 52.7, $p=0.046$) (Fig. 6F). The proportion of GFP-MSCs in GFP-positive cells did not show significant difference between the MSC systemic injection group and the MSC local injection group ($30.69 \pm 10.01\%$ vs. $26.74 \pm 10.66\%$, $p=0.609$) (Fig. 6G). The proportion of GFP-osteoblasts in GFP-positive cells in the MSC systemic injection group was significantly lower than that

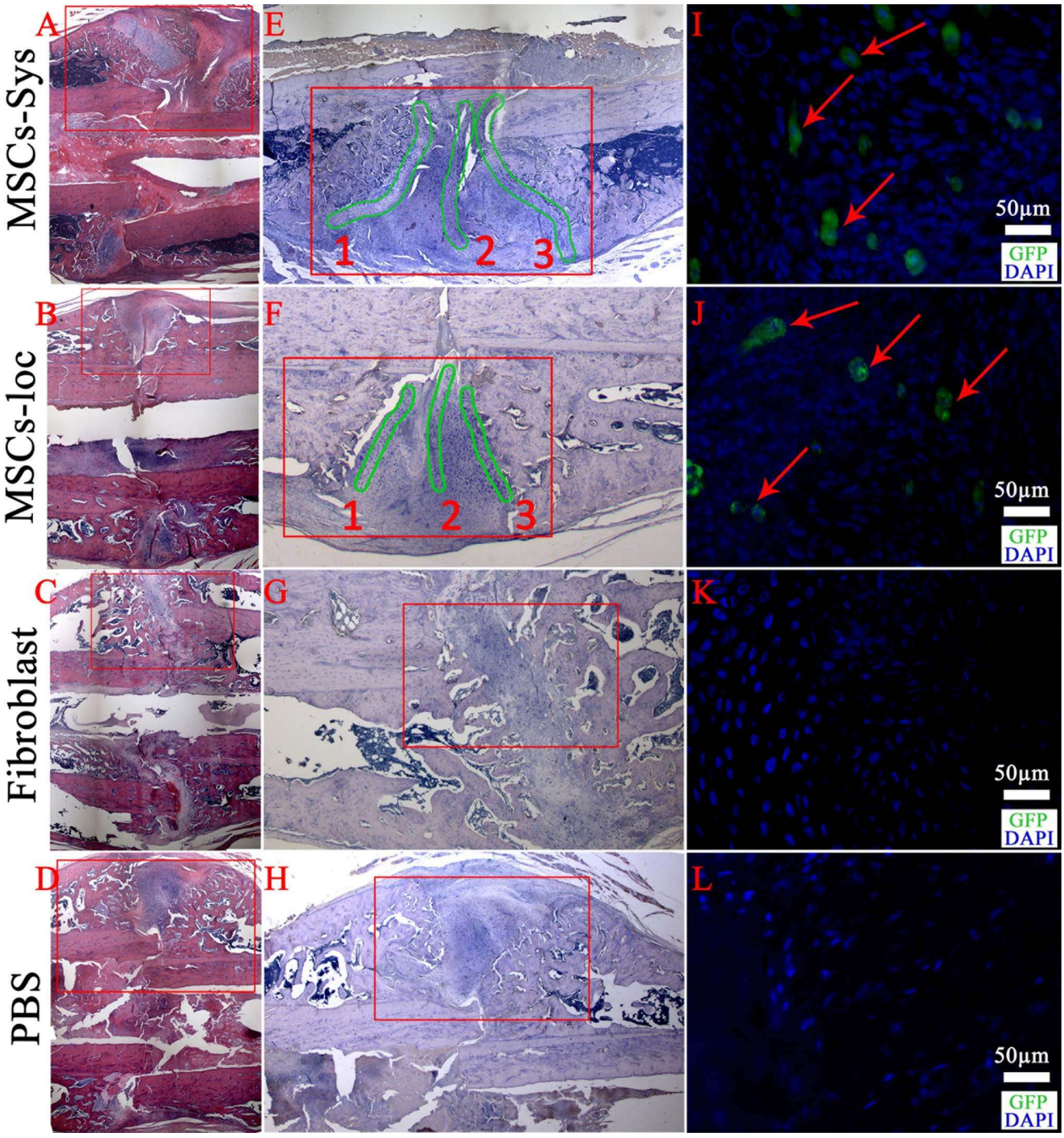

Figure 4. H&E staining, HRP-DAB, and immunofluorescence staining for GFP. (A–D) The fractured bone sections were stained with H&E. (E–H) HRP-DAB immunostaining was carried out for detecting GFP-positive cells; high-resolution images were enlarged from the red outlined areas in (A–D). (E, F) GFP-positive cells (brown cells) were found in the MSC-sys group and the MSC-loc group at 5 weeks following the fracture. GFP-positive cells mainly distributed within the three green outlined areas in the MSC systemic and local injection groups. (G, H) None of GFP-positive cells were found in the fibroblast and PBS injection group. (I–L) Immunofluorescence micrographs of fractured bone sections stained for GFP (FITC immunolabeling) and DAPI (blue); high-resolution images were enlarged from the red outlined areas in (E–H). (I, J) GFP-positive cells (green cells pointed out by red arrows) were found in the MSC-sys group and MSC-loc group at 5 weeks following the fracture. (K, L) None of GFP-positive cells were found in the fibroblast and PBS injection group. Scale bar: 50 μm.

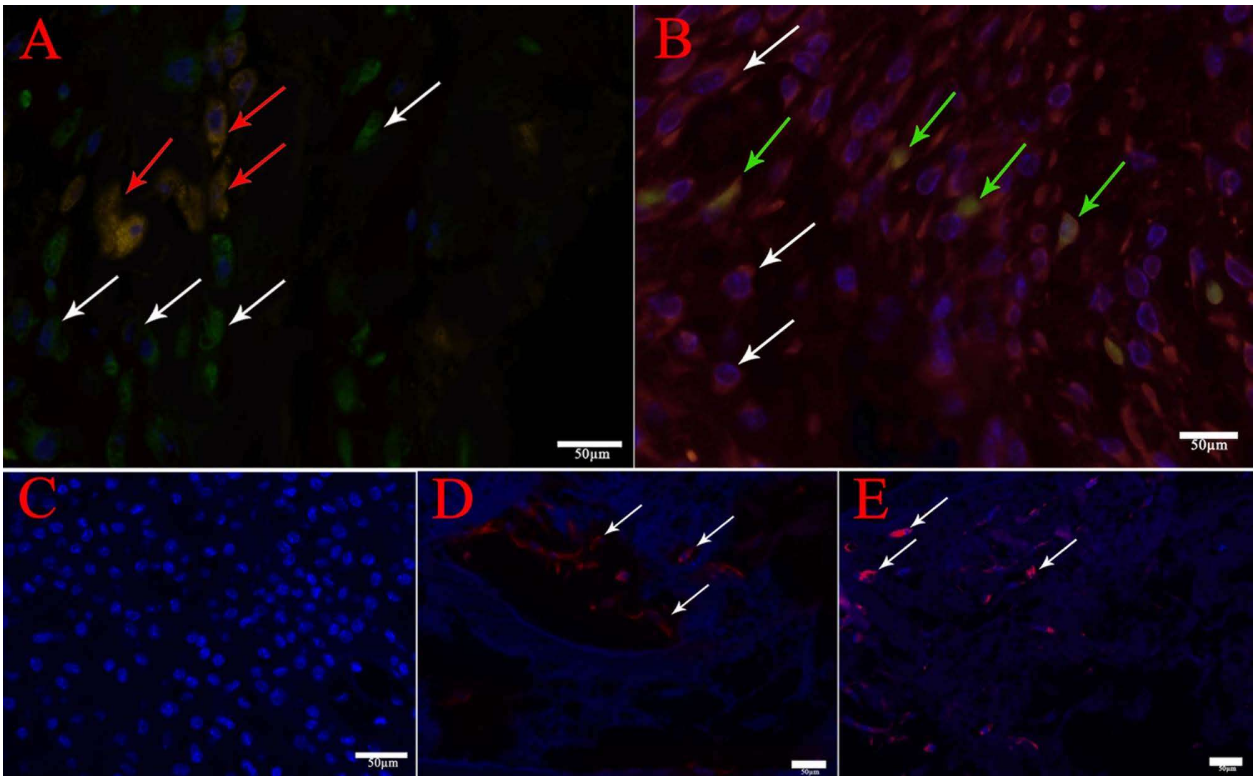

Figure 5. Images of double immunofluorescence staining for GFP and nestin (DAPI for nuclei). In order to examine the codistribution of GFP (FITC immunolabeling) and nestin (Cy3 immunolabeling) in the same sample, a double immunofluorescence staining was carried out in the same section. (A) $GFP^+/nestin^+$ MSCs, the red-yellow cells pointed out by the red arrows, were observed in the MSC systemic injection group at 5 weeks following the fracture. $GFP^+/nestin^-$ cells, the green cells pointed out by the white arrows were also observed. (B) $GFP^+/nestin^+$ MSCs (green arrows) and $GFP^-/nestin^+$ MSCs (white arrows) were both observed in the MSC local injection group at 5 weeks following the fracture. (C–E) GFP-positive cells (green cells) were not found in the antibody negative control group (C), the PBS control group (D), and the fibroblast group (E), but $GFP^-/nestin^+$ MSCs (red cells pointed out by white arrows) were found in both the PBS control group (D) and the fibroblast group (E). Scale bar: 50 μm.

of the MSC local injection group ($20.60 \pm 11.30\%$ vs. $37.96 \pm 4.83\%$, $p = 0.030$) (Fig. 6H).

DISCUSSION

MSCs have been used for cell therapies in various disease models. However, questions still remain. For example, should we use autologous or allogeneic MSCs? Local injection versus systemic injection, which routine is better? What are the roles of MSCs engrafted at the injurious sites?

The application of MSCs in augmenting bone formation have been studied and reported, most on the use of autologous MSCs and some on the use of allogeneic MSCs. The use of allogeneic MSCs is still a controversial issue, as there are concerns of immune rejection and inflammation that the allogeneic MSCs may cause. In contrast to the use of autologous MSCs, allogeneic MSCs can be well prepared in advance, independent from the receiver's age and disease status, and can be banked and used as off-the-shelf medical products.

The current study has demonstrated that allogeneic MSCs through either systemic or local injection could promote fracture repair significantly in the rat fracture model, and neither of them elicited any obvious immune responses in this study. This is the first report to compare the use of allogeneic MSCs locally or systemically in fracture healing shoulder by shoulder and provide some insights on the use of allogeneic MSCs in promoting fracture healing. In normal situations, local application shall be the first choice, whereas in difficult conditions such as multiple fractures, the use of systemic administration may be the desired choice.

In this study, we used heart injection of MSCs instead of intravenous injection through the tail vein. The blood vessels in the rat tail vein are thin, so some cells may leak out from the vein, and it is hard to be sure an equal number of cells were injected into the experimental animals. Our pilot data from in vivo imaging analysis showed that in both heart injection and intravenous injection, the injected GFP-MSCs go to the lungs within minutes of

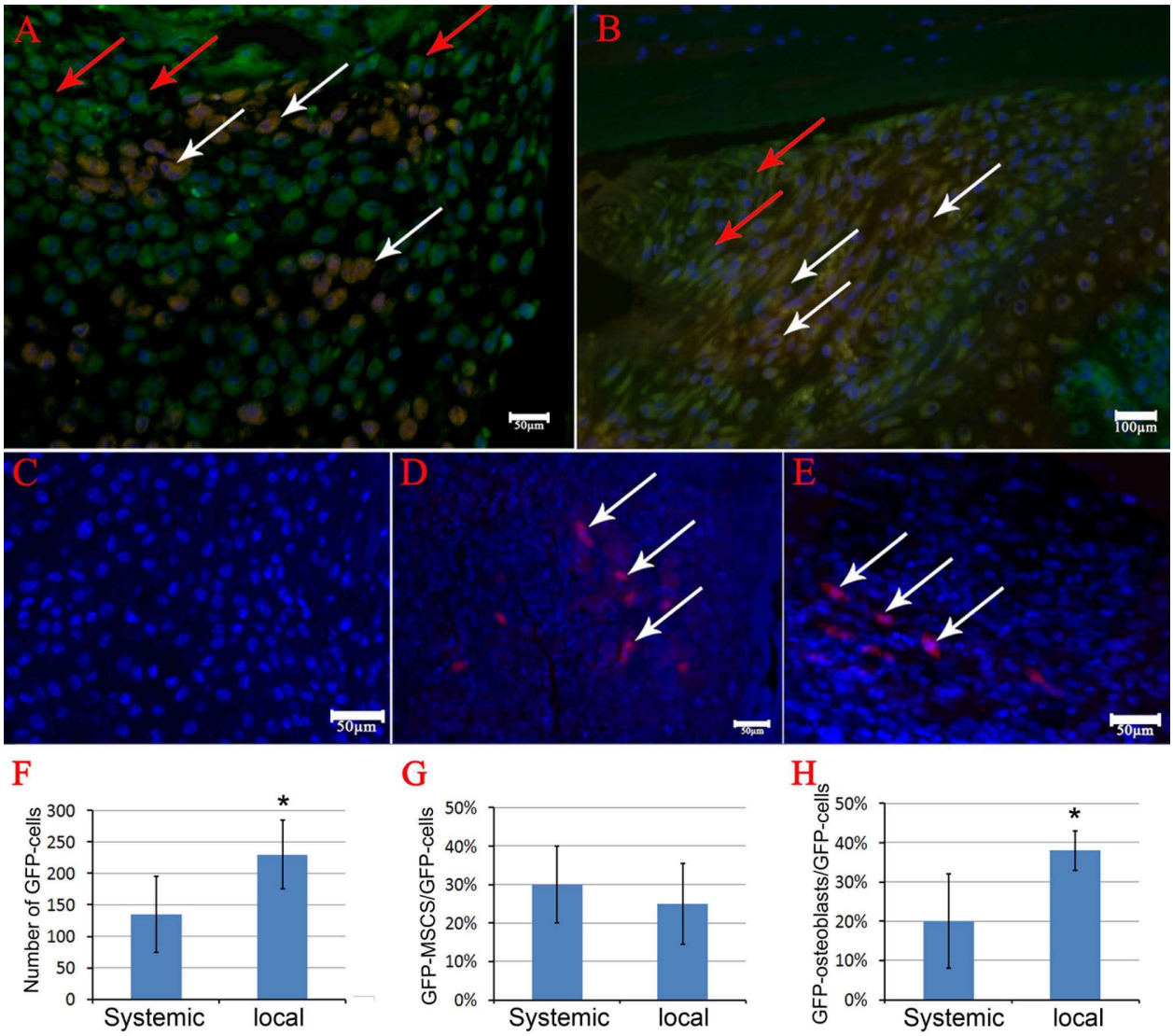

Figure 6. Images of double immunofluorescence staining for GFP and osterix (DAPI for nuclei). Double immunofluorescence staining of GFP (FITC immunolabeling) and osterix (Cy3 immunolabeling), which is a transcription factor for osteoblasts, was carried out in the same sample. (A, B) $GFP^+/osterix^+$ osteoblasts (the red-yellow cells pointed out by white arrows) were observed in both the MSC systemic injection group (A) and the MSC local injection group (B) at 5 weeks following the fracture; $GFP^+/osterix^-$ cells (the green cells pointed out by red arrows) were also found in both MSC injection groups. (C–E) GFP-positive cells (green cells) were not found in the antibody negative control (C), the PBS control group (D), and the fibroblast group (E), but $GFP^-/osterix^+$ osteoblasts (red cells pointed out by white arrows) were found both in the PBS control group (D) and the fibroblast group (E) at 5 weeks following the fracture. (F) Quantitative analysis showed that the number of MSCs migrated into the injury sites following systemic injection was less than that of the local injection group ($p=0.046$). (G) The proportion of GFP-MSCs in GFP-positive cells did not show significant difference between the MSC-sys and MSC-loc injection group ($p=0.609$). (H) The proportion of GFP osteoblasts in GFP-positive cells in the MSC-sys group was significantly lower than that of the MSC-loc group ($p=0.030$). Scale bar: 50 μm.

injection and are retained there for about 6–7 days then redistributed throughout the body.

As to the cellular and molecular mechanisms of how the engrafted MSCs promote the fracture healing, there may be two possible answers. 1) MSCs could directly contribute to the bone repair. Some researchers supported that MSCs possess multidifferentiation potential; therefore, they mediate tissue and organ repair by replacing damaged cells (26,28). In this rat fracture model, our immunofluorescence staining results showed that both systemically and locally injected GFP-MSCs were able to differentiate into osteoblasts to directly participate in bone formation at 5 weeks following the fracture. 2) MSCs may also indirectly contribute to the bone repair through

regulating inflammation and/or releasing growth factors/cytokines at the fracture sites (3,9,17–19). Le Blanc and colleagues showed that MSCs can suppress the proliferation of both $CD4^+$ and $CD8^+$ T cells by upregulating the release of soluble factors, such as interleukin-10 and prostaglandin E2 (21). Kellie and colleagues found that MSC treatment increases the tensile strength of wounds and are associated with increased productions and depositions of structural collagen in the wound (27). In 2009, Granero-Molto et al. reported that transplanted allogeneic MSCs improve the mouse fracture repair process through expressing bone morphogenetic protein-2 (BMP-2) at the fracture site (16). MSCs may secrete paracrine factors such as BMP-2 to enhance osteogenesis, vascular endothelial growth factor (VEGF), and angiopoietin-1 to enhance angiogenesis or reduce inflammation through regulating apoptosis and immune cell proliferation at the fracture site (7,8,36,37).

Systemic injection is more advisable for treatment of injuries involving deeper or multiple sites, while local injection is simpler for single and superficial injuries. In the current study, both groups with MSC administration work equally well in promoting fracture healing, and the reasons could be 1) limited sample size used in the current study may not verify the small difference; 2) both routes of MSC administration work equally well in promoting fracture healing in the rat fracture model; 3) a high dose of systemically injected cells ensured enough cells migrated to the fracture site, hence diminished the difference; 4) some systemically injected cells may contribute to the fracture healing in indirect ways such as immune modulation.

Our immunofluorescence staining results showed that both locally and systemically injected MSCs were present in the callus, suggesting that some allogeneic MSCs could survive and maintain their phenotype for at least 5 weeks in vivo. Our quantitative analysis data showed that the number of GFP-positive cells that migrated into the injury sites following the systemic injection were significantly less than that of the local injection group. It is well understood that after systemic injection, MSCs distributed into the whole body through the blood circulation, and many of them were trapped in the microvasculature (blood barrier) of the lungs, but those MSCs could redistribute in a few days to the site of injuries; therefore, the cell numbers seen at the fracture site in the systemic injection group were lower. Nonetheless, the cells that reached the fracture site in the systemic injection group all come through the vascular network, and because they are close to the circulatory network, they shall survive and function well. In contrast, the locally injected cells may not all survive and function well as they are passively injected into the compromised local environment. Injury sites usually ensure low pH, poor blood supply, hypoxia, inflammation, and infection, etc.

Our data also showed that the proportion of GFP osteoblasts in the GFP-positive cells in the MSC systemic injection group was significantly lower than that of the MSC local injection group, indicating that systemically injected cells may contribute more to the fracture healing in indirect ways. For instance, they may regulate the immune cells through cell–cell interactions and reduce the inflammatory reactions following injuries, and mobilize autologous MSCs to home, proliferate, and differentiate at the injury sites. Therefore, systemic administration of allogenic MSCs may have advantages over local MSC administration due to its roles in immune regulations and promoting functions of autologous MSCs. The underlying mechanisms of action still need careful investigation.

In conclusion, our data in the current study showed that systemic and local administration of allogeneic MSCs promoted rat fracture healing by enhancing callus formation and their mechanical properties with no obvious adverse effects. The use of allogenic MSC administration may have clinical implications in managing serious and multiple tissue injuries. However, many questions are still unanswered. For example, do these GFP-MSCs at the fracture sites release growth factors/cytokines to regulate inflammation and promote bone healing? What are the cellular and molecular mechanisms behind the therapeutic effects? Do systemically and locally injected MSCs promote fracture healing through different mechanisms? Future studies are needed to address the exact cellular and molecular mechanisms behind the allogeneic MSC administration in promoting fracture repair.

ACKNOWLEDGMENTS: This work is supported by a grant from the Hong Kong Government Research Grant Council, General Research Fund (CUHK470813), and a grant from China Shenzhen City Science and Technology Bureau under the Shenzhen City Knowledge Innovation Plan, Basic Research Project (JCYJ20130401171935811) to Gang Li. This study was also supported in part by the SMART program, Lui Che Woo Institute of Innovative Medicine, Faculty of Medicine, The Chinese University of Hong Kong. This research project was made possible by resources donated by Lui Che Woo Foundation Limited. We also acknowledge the generous support of Li Ka Shing Institute to allow us to use the GMP cell culture facility to make this study possible. The authors declare no conflicts of interest.

REFERENCES

1. Abd El-Salam, M. M.; Al-Ghitany, E. M.; Kassem, M. M. Quality of bottled water brands in Egypt part II: Biological water examination. J. Egypt Public Health Assoc. 83(5–6):468–486; 2008.
2. Bang, O. Y.; Lee, J. S.; Lee, P. H.; Lee, G. Autologous mesenchymal stem cell transplantation in stroke patients. Ann. Neurol. 57(6):874–882; 2005.
3. Block, G. J.; Ohkouchi, S.; Fung, F.; Frenkel, J.; Gregory, C.; Pochampally, R.; DiMattia, G.; Sullivan, D. E.; Prockop, D. J. Multipotent stromal cells are activated to

reduce apoptosis in part by upregulation and secretion of stanniocalcin-1. Stem Cells 27(3):670–681; 2009.
4. Bruder, S. P.; Kraus, K. H.; Goldberg, V. M.; Kadiyala, S. The effect of implants loaded with autologous mesenchymal stem cells on the healing of canine segmental bone defects. J. Bone Joint Surg. Am. 80(7):985–996; 1998.
5. Bruder, S. P.; Kurth, A. A.; Shea, M.; Hayes, W. C.; Jaiswal, N.; Kadiyala, S. Bone regeneration by implantation of purified, culture-expanded human mesenchymal stem cells. J. Orthop. Res. 16(2):155–162; 1998.
6. Campagnoli, C.; Roberts, I. A.; Kumar, S.; Bennett, P. R.; Bellantuono, I.; Fisk, N. M. Identification of mesenchymal stem/progenitor cells in human first-trimester fetal blood, liver, and bone marrow. Blood 98(8):2396–2402; 2001.
7. Cao, L.; Liu, X.; Liu, S.; Jiang, Y.; Zhang, X.; Zhang, C.; Zeng, B. Experimental repair of segmental bone defects in rabbits by angiopoietin-1 gene transfected MSCs seeded on porous beta-TCP scaffolds. J. Biomed. Mater. Res. B Appl. Biomater. 100(5):1229–1236; 2012.
8. Chan, J. K.; Lam, P. Y. Human mesenchymal stem cells and their paracrine factors for the treatment of brain tumors. Cancer Gene Ther. 20(10):539–543; 2013.
9. Chen, L.; Tredget, E. E.; Wu, P. Y.; Wu, Y. Paracrine factors of mesenchymal stem cells recruit macrophages and endothelial lineage cells and enhance wound healing. PLoS One 3(4):e1886; 2008.
10. Chen, S. L.; Fang, W. W.; Ye, F.; Liu, Y. H.; Qian, J.; Shan, S. J.; Zhang, J. J.; Chunhua, R. Z.; Liao, L. M.; Lin, S.; Sun J. P. Effect on left ventricular function of intracoronary transplantation of autologous bone marrow mesenchymal stem cell in patients with acute myocardial infarction. Am. J. Cardiol. 94(1):92–95; 2004.
11. Cheung, W. H.; Sun, M. H.; Zheng, Y. P.; Chu, W. C.; Leung, A. H.; Qin, L.; Wei, F. Y.; Leung, K. S. Stimulated angiogenesis for fracture healing augmented by low-magnitude, high-frequency vibration in a rat model-evaluation of pulsed-wave doppler, 3-D power Doppler ultrasonography and micro-CT microangiography. Ultrasound Med. Biol. 38(12):2120–2129; 2012.
12. Cole, J. H.; van der Meulen, M. C. Whole bone mechanics and bone quality. Clin. Orthop. Relat. Res. 469(8):2139–2149; 2011.
13. Devine, M. J.; Mierisch, C. M.; Jang, E.; Anderson, P. C.; Balian, G. Transplanted bone marrow cells localize to fracture callus in a mouse model. J. Orthop. Res. 20(6):1232–1239; 2002.
14. Erices, A.; Conget, P.; Minguell, J. J. Mesenchymal progenitor cells in human umbilical cord blood. Br. J. Haematol. 109(1):235–242; 2000.
15. Gaur, T.; Lengner, C. J.; Hovhannisyan, H.; Bhat, R. A.; Bodine, P. V.; Komm, B. S.; Javed, A.; van Wijnen, A. J.; Stein, J. L.; Stein, G. S.; Lian, J. B. Canonical WNT signaling promotes osteogenesis by directly stimulating Runx2 gene expression. J. Biol. Chem. 280(39):33132–33140; 2005.
16. Granero-Molto, F.; Weis, J. A.; Miga, M. I.; Landis, B.; Myers, T. J.; O'Rear, L.; Longobardi, L.; Jansen, E. D.; Mortlock, D. P.; Spagnoli, A. Regenerative effects of transplanted mesenchymal stem cells in fracture healing. Stem Cells 27(8):1887–1898; 2009.
17. Karp, J. M.; Leng Teo, G. S. Mesenchymal stem cell homing: The devil is in the details. Cell Stem Cell 4(3):206–216; 2009.
18. Kassem, M.; Abdallah, B. M. Human bone-marrow-derived mesenchymal stem cells: Biological characteristics and potential role in therapy of degenerative diseases. Cell Tissue Res. 331(1):157–163; 2008.
19. Koc, O. N.; Day, J.; Nieder, M.; Gerson, S. L.; Lazarus, H. M.; Krivit, W. Allogeneic mesenchymal stem cell infusion for treatment of metachromatic leukodystrophy (MLD) and Hurler syndrome (MPS-IH). Bone Marrow Transplant. 30(4):215–222; 2002.
20. Le Blanc, K. Immunomodulatory effects of fetal and adult mesenchymal stem cells. Cytotherapy 5(6):485–489; 2003.
21. Le Blanc, K.; Tammik, L.; Sundberg, B.; Haynesworth, S. E.; Ringden, O. Mesenchymal stem cells inhibit and stimulate mixed lymphocyte cultures and mitogenic responses independently of the major histocompatibility complex. Scand. J. Immunol. 57(1):11–20; 2003.
22. Lee, J. S.; Hong, J. M.; Moon, G. J.; Lee, P. H.; Ahn, Y. H.; Bang, O. Y. A long-term follow-up study of intravenous autologous mesenchymal stem cell transplantation in patients with ischemic stroke. Stem Cells 28(6):1099–1106; 2010.
23. Lee, R. H.; Seo, M. J.; Reger, R. L.; Spees, J. L.; Pulin, A. A.; Olson, S. D.; Prockop, D. J. Multipotent stromal cells from human marrow home to and promote repair of pancreatic islets and renal glomeruli in diabetic NOD/scid mice. Proc. Natl. Acad. Sci. USA 103(46):17438–17443; 2006.
24. Leung, K. S.; Shi, H. F.; Cheung, W. H.; Qin, L.; Ng, W. K.; Tam, K. F.; Tang, N. Low-magnitude high-frequency vibration accelerates callus formation, mineralization, and fracture healing in rats. J. Orthop. Res. 27(4):458–465; 2009.
25. Livingston, T. L.; Gordon, S.; Archambault, M.; Kadiyala, S.; McIntosh, K.; Smith, A.; Peter, S. J. Mesenchymal stem cells combined with biphasic calcium phosphate ceramics promote bone regeneration. J. Mater. Sci. Mater. Med. 14(3):211–218; 2003.
26. Mahmood, A.; Lu, D.; Lu, M.; Chopp, M. Treatment of traumatic brain injury in adult rats with intravenous administration of human bone marrow stromal cells. Neurosurgery 53(3):697–702; discussion 702–703; 2003.
27. McFarlin, K.; Gao, X.; Liu, Y. B.; Dulchavsky, D. S.; Kwon, D.; Arbab, A. S.; Bansal, M.; Li, Y.; Chopp, M.; Dulchavsky, S. A.; Gautam, S. C. Bone marrow-derived mesenchymal stromal cells accelerate wound healing in the rat. Wound Repair Regen. 14(4):471–478; 2006.
28. Murphy, J. M.; Fink, D. J.; Hunziker, E. B.; Barry, F. P. Stem cell therapy in a caprine model of osteoarthritis. Arthritis Rheum. 48(12):3464–3474; 2003.
29. Ortiz, L. A.; Dutreil, M.; Fattman, C.; Pandey, A. C.; Torres, G.; Go, K.; Phinney, D. G. Interleukin 1 receptor antagonist mediates the antiinflammatory and antifibrotic effect of mesenchymal stem cells during lung injury. Proc. Natl. Acad. Sci. USA 104(26):11002–11007; 2007.
30. Ortiz, L. A.; Gambelli, F.; McBride, C.; Gaupp, D.; Baddoo, M.; Kaminski, N.; Phinney, D. G. Mesenchymal stem cell engraftment in lung is enhanced in response to bleomycin exposure and ameliorates its fibrotic effects. Proc. Natl. Acad. Sci. USA 100(14):8407–8411; 2003.
31. Parekkadan, B.; van Poll, D.; Suganuma, K.; Carter, E. A.; Berthiaume, F.; Tilles, A. W.; Yarmush, M. L. Mesenchymal stem cell-derived molecules reverse fulminant hepatic failure. PLoS One 2(9):e941; 2007.
32. Pittenger, M. F.; Mackay, A. M.; Beck, S. C.; Jaiswal, R. K.; Douglas, R.; Mosca, J. D.; Moorman, M. A.; Simonetti, D. W.; Craig, S.; Marshak, D. R. Multilineage

potential of adult human mesenchymal stem cells. Science 284(5411):143–147; 1999.
33. Sanchez-Ramos, J. R. Neural cells derived from adult bone marrow and umbilical cord blood. J. Neurosci. Res. 69(6):880–893; 2002.
34. Shirley, D.; Marsh, D.; Jordan, G.; McQuaid, S.; Li, G. Systemic recruitment of osteoblastic cells in fracture healing. J. Orthop. Res. 23(5):1013–1021; 2005.
35. Xu, L. L.; Li, G. Circulating mesenchymal stem cells and their clinical implications. J. Orth. Transl. (2): 1–7; 2014.
36. Zhang, T.; Lee, Y. W.; Rui, Y. F.; Cheng, T. Y.; Jiang, X. H.; Li, G. Bone marrow-derived mesenchymal stem cells promote growth and angiogenesis of breast and prostate tumors. Stem Cell Res. Ther. 4(3):70; 2013.
37. Zhou, Y.; Guan, X.; Yu, M.; Wang, X.; Zhu, W.; Wang, C.; Yu, M.; Wang, H. Angiogenic/osteogenic response of BMMSCs on bone-derived scaffold: Effect of hypoxia and role of PI3K/Akt-mediated VEGF-VEGFR pathway. Biotechnol. J. 9(7):944–953; 2014.